The influence of extratropical cross-tropopause mixing on the correlation between ozone and sulfate aerosol in the lowermost stratosphere

Philipp Joppe[1,2], Johannes Schneider[2], Katharina Kaiser[1,2], Horst Fischer[3], Peter Hoor[1], Daniel Kunkel[1], Hans-Christoph Lachnitt[1], Andreas Marsing[4], Lenard Röder[3], Hans Schlager[4], Laura Tomsche[1,4], Christiane Voigt[1,4], Andreas Zahn[5], and Stephan Borrmann[1,2]

[1]Institute for Atmospheric Physics, Johannes Gutenberg University Mainz, Germany
[2]Particle Chemistry Department, Max Planck Institute for Chemistry, Mainz, Germany
[3]Atmospheric Chemistry Department, Max Planck Institute for Chemistry, Mainz, Germany
[4]Institute of Atmospheric Physics, Deutsches Zentrum für Luft- und Raumfahrt (DLR), Oberpfaffenhofen, Germany
[5]Karlsruhe Institute of Technology, Institute of Meteorology and Climate Research, Karlsruhe, Germany

Correspondence: Philipp Joppe (phjoppe@uni-mainz.de)

Abstract. The composition of the upper troposphere/lower stratosphere region (UTLS) is influenced by horizontal transport, vertical transport within convective systems and warm conveyor belts, rapid turbulent mixing, as well as photochemical production or loss of species. This results in the formation of the extratropical transition layer (ExTL), which has been defined by the vertical structure of CO profiles and studied by now mostly by means of trace gas correlations. Here, we extend the analysis
5 to aerosol particles and derive the ozone to sulfate aerosol correlation in Central Europe from aircraft in-situ measurements during the CAFE-EU/BLUESKY mission, probing the UTLS during the COVID-19 period with significant reduced anthropogenic emissions. We operated a compact time-of-flight aerosol mass spectrometer (C-ToF-AMS) to measure the chemical composition of non-refractory aerosol particles in the size range from about 40 to 800 nm. In our study, we find a correlation between the ozone mixing ratio (O_3) and the sulfate mass concentration in the lower stratosphere. The correlation exhibits
10 some variability over the measurement period exceeding the background sulfate to ozone correlation. Especially during one flight, we observed enhanced mixing ratios of sulfate aerosol in the lowermost stratosphere, where the analysis of trace gases shows tropospheric influence. Also, back trajectories indicate, that no recent mixing with tropospheric air occurred within the last 10 days. In addition, we analyzed satellite SO_2 retrievals from TROPOMI for volcanic plumes and eruptions. From these analyses, we conclude that gas-to-particle conversion of volcanic SO_2 leads to the observed enhanced sulfate aerosol mixing
15 ratios.

1 Introduction

The chemical composition of upper tropospheric aerosol particles is highly variable because primary aerosols from natural and anthropogenic ground sources reach this altitude (Martinsson et al., 2019), and secondary aerosols are formed here from gas-to-particle conversion. However, the stratospheric aerosol composition is less complex as the main component is particu-

20 late sulfate (SO_4^{2-}) with concentrations between 0.1 and 40 µg m^{-3} accompanied by minor tropospheric compounds (Deshler, 2008; Murphy et al., 2013; Brimblecombe, 2014; Kremser et al., 2016).

The stratospheric aerosol layer, also known as "Junge layer" (Junge and Manson, 1961), is part of the lowermost stratosphere (LMS) and is located roughly between 15 and 25 km (Hofmann and Rosen, 1981). The chemical composition of the aerosol layer underlies seasonal variations induced by the Brewer-Dobson circulation (Martinsson, 2005; Friberg et al., 2014) and

25 volcanic activity, which may increase the aerosol optical depth (AOD) by up to 40 % (Friberg et al., 2018). Sulfate aerosol is formed due to oxidation of carbonyl sulfide (OCS) and sulfur dioxide (SO_2) (Crutzen, 1976; Brühl et al., 2012; Solomon et al., 2011; Kremser et al., 2016). Both precursor gases have their main sources in the troposphere. OCS is the main sulfur containing trace gas in the atmosphere and has biological sources, such as photochemical dissolving of organic matter and oceanic emissions (Andreae, 1990; Brühl et al., 2012; Kremser et al., 2016). SO_2 is primary emitted by industrial processes like the fossil

30 fuel burning. While degassing volcanoes contribute to the tropospheric SO_2 budget (Voigt et al., 2014), explosive eruptions can directly inject SO_2 into the lower stratosphere (Kremser et al., 2016). Another direct sulfate aerosol source are aircraft which emit soot and volatile sulfate containing particles at cruise altitudes into the upper troposphere/lower stratosphere (Voigt et al., 2010; Williamson et al., 2021; Tomsche et al., 2022).

Transport processes of aerosol particles into the UTLS have been subject of several studies, for example with focus on tropical

35 processes or the Asian tropopause aerosol layer (ATAL) (e.g., Appel et al., 2022; Fadnavis et al., 2013; Froyd et al., 2009; Höpfner et al., 2019). Tracer correlations of aerosol particles with ozone (O_3) and nitrous oxide (N_2O) based on high altitude in-situ measurements also have been used in the context of polar vortex dynamics after a major volcanic eruption (Borrmann et al., 1993, 1995). In those studies, the temporal evolution of the correlation between the mixing ratios of sulfate aerosol, surface area for aerosol particles with a size between roughly 10 nm and more than one µm, in addition to O_3 inside and out-

40 side of the polar vortex was analyzed over the course of 22 months after the Mt. Pinatubo eruption in 1991. The observations revealed a slow development of a linear correlation between the O_3 versus aerosol number and surface mixing ratios in the mid latitude UTLS, which degraded again later on. This demonstrated the suitability of aerosol properties as dynamical tracers once the microphysical processes like new particle formation, coagulation, and condensational growth following a volcanic eruption into the stratosphere have ceased. Furthermore, a temporally stable equilibrium of particle size/surface area has been

45 established.

In the extratropics, the chemical composition of the tropopause region is influenced not only by the Brewer-Dobson circulation, but also by convection, mixing along the subtropical and polar frontal jet streams, breaking of gravity and Rossby waves, and vertical wind shear (e.g., Gettelman et al., 2011; Kaluza et al., 2021). This forms a transition layer above the tropopause, called the extratropical transition layer (ExTL), where tropospheric as well as stratospheric influence is observed (Hoor et al.,

50 2004; Hegglin et al., 2009; Gettelman et al., 2011; Konopka and Pan, 2012; Barré et al., 2013). The effect of these small-scale mixing processes on the chemical composition of aerosol particles in the ExTL is not well known until now (Kunkel et al., 2019). The lifetime of atmospheric aerosol particles with diameters lower than one µm can reach one month or more (Jaenicke, 1980). This is sufficient for the particles to be transported up into the tropopause region over long distances and subsequently, by mixing processes, into the stratosphere. Furthermore, the lifetime of more than a month corresponds to the timescale that

55 gas-to-particle conversion needs to form sulfate aerosol particles from SO_2 as a precursor gas in the UTLS (Jurkat et al., 2010; Gorkavyi et al., 2021; Rollins et al., 2017).

In our study, we use tracer-tracer correlations as a tool for mixing diagnostics to identify stratospheric air masses and underlying mixing processes. The basic principle of this method is to use a tropospheric tracer with sources in the troposphere and a rather constant stratospheric background, e.g. carbon monoxide (CO) and water vapor (H_2O), and a tracer with only a

60 stratospheric increase or decrease and a fairly constant mixing ratio in the troposphere, e.g. O_3 or N_2O. In a scatter plot with the tropospheric tracer on the abscissa and the stratospheric tracer on the ordinate, one would expect two separated reservoirs that are not connected if no mixing processes would occur. If mixing takes place, both reservoirs are be connected by mixing lines, where the mixing ratios are between the two regimes, depending on the state of mixing (Fischer et al., 2000; Hoor et al., 2002).

65 With this study we want to introduce particulate sulfate as stratospheric tracer in the correlation with O_3 and find processes that are responsible for the variability of the correlation between sulfate aerosol and O_3 mixing ratios. Therefore, we use in-situ aircraft measurements from the CAFE-EU (Chemistry of the Atmosphere Field Experiment over Europe)/BLUESKY mission, conducted in spring 2020 from Oberpfaffenhofen, Germany.

70 ## 2 Methods

2.1 Data overview

The CAFE-EU/BLUESKY measurement campaign was conducted with the research aircraft HALO (High Altitude and Long Range Research Aircraft) and DLR-Falcon, both operated by the German Aerospace Center (DLR). The measurement flights were performed over Central Europe and the North Atlantic between 16 May and 09 June 2020, partly co-located with both

75 aircraft (see Fig. 1). The measurements were conducted during the first COVID-19 lockdown in Germany and Europe, such that the main goal of the campaign was to investigate the atmospheric changes during reduced industrial activity and lower emissions compared to other times (Voigt et al., 2022). During this time, air traffic was significantly reducd over Europe by up to 80 % (Schumann et al., 2021a, b). Krüger et al. (2022) found substantial reduction in aerosol particles in the lower troposphere in this period and Reifenberg et al. (2022) could explain the observed reduction in some tracer concentrations with the reduced

80 emissions of pollutants. Tomsche et al. (2022) investigated the SO2 concentrations in the UTLS region above Europe, which was influenced by changes in sulfur sources such as aviation as well as sinks. Here we focus on the transport processes in the extratropical transition layer, which has been probed with a set of instrumentations onboard HALO and DLR-Falcon.

2.2 Instrumentation

For our study, we use the chemical composition of aerosol particles measured onboard HALO and trace gas measurements
85 onboard HALO and DLR-Falcon. The chemical composition of non-refractory aerosol particles was measured on HALO with
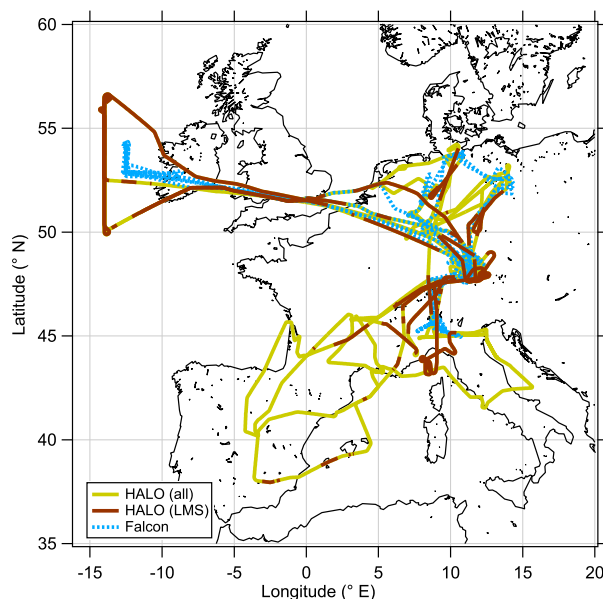
Figure 1. Overview map of all measurement flights performed during the CAFE-EU/BLUESKY measurement campaign between 16 May and 09 June 2020. The HALO flight path as solid line divided into the complete data set (yellow) and stratospheric (brown) segments, while the DLR-Falcon flight path is shown as a dashed blue line.

a compact time-of-flight aerosol mass spectrometer (C-ToF-AMS) for particles in the size range between 40 nm and 800 nm (Drewnick et al., 2005; Schulz et al., 2018) and with this within the same size range as previous studies (e.g., Borrmann et al., 1995). We obtain quantitative information on the mass concentration of sulfate, nitrate, ammonium, organic matter and chloride normalized to STP conditions. The measurement interval of the C-ToF-AMS during the campaign was 30 s, resulting in a spatial resolution of about 6 km in the UTLS region. The accuracy of the AMS is about 30 % (Canagaratna et al., 2007; Middlebrook et al., 2012). In the following, we use the mixing ratio instead of the mass concentration for comparison with the trace gas measurements

In addition to the aerosol chemical composition data, we use trace gas measurements, like SO_2, CO, H_2O, O_3 and nitric acid (HNO_3) onboard HALO and DLR-Falcon.

CO measurements on HALO were performed with the quantum cascade laser absorption spectrometer TRISTAR (Tadic et al., 2017; Röder et al., 2023) with a total measurement uncertainty of 3 % at 10 s time resolution. O_3 on HALO was measured by FAIRO which measured on the basis of a UV photometer and chemiluminescence (Zahn et al., 2011). On board the DLR-Falcon, CO and O_3 were measured with a cavity ring-down spectrometer (PICARRO G2401) and a dual-cell UV photometer (TE 49C), respectively. Both instruments were calibrated before and after the flights with standards that can be traced back to the GAW Station Hohenpeissenberg. The precision/accuracy of the CO and O_3 measurements are 3 ppbv/ 5 ppbv and 3 %/ 5%, respectively. An additional in-situ data set is provided by the atmospheric chemical ionization mass spectrometer (AIMS) deployed on DLR-Falcon and includes information on gaseous SO_2 and HNO_3. For the detection of upper tropospheric and

lower stratospheric SO_2 and HNO_3 mixing ratios the AIMS uses SF_5^- reagent ions (Voigt et al., 2014; Jurkat et al., 2016; Marsing et al., 2019; Tomsche et al., 2022). The one sigma detection limit is 0.0006 to 0.0017 ppbv and 0.005 to 0.009 ppbv

105 for SO_2 and HNO_3, respectively. The total uncertainty for SO_2 is 22.7 % (Tomsche et al., 2022) and 16 % for HNO_3 (Marsing, 2021).

2.3 Meteorology and trajectories

In addition to the in-situ measurement data, we use model data interpolated onto the flight path of both aircraft. For meteorological information, we use the ERA5 reanalysis data set with a temporal resolution of three hours and a grid spacing of

110 $0.5°$ in the horizontal and a vertical spacing of approximately 500 m in the UTLS (Hersbach et al., 2020). Based on the native variables we additionally calculated potential vorticity and equivalent latitude.

For our analysis of the air mass origin and possible transport pathways, we use trajectories calculated with the Lagrangian analysis tool (LAGRANTO; Sprenger and Wernli, 2015). Therefore, we initialize a set of trajectories every 30 seconds along the flight path. The starting points of the trajectories of each set are placed in a three dimensional box around the actual point

115 at the flight path, to gain a better statistic and to minimize interpolation errors between the measurements and the model grid. More specifically, we take the location of the aircraft and add five additional points every 0.01 degree in all horizontal directions and five points every one hPa above and below the altitude of the aircraft. Thus, a total of 231 trajectories are started at each release time, providing information for 10 days back in time with quantities such as potential temperature and potential vorticity.

120 # 3 Results

3.1 Part 1: Correlation of ozone and particulate sulfate

O_3 is a suitable tracer to identify stratospheric air masses due to the photochemical production of O_3 in the stratosphere and its low abundance in the troposphere and its local chemical lifetime of years in the lower stratosphere. There are several ways to identify the tropopause and thus the lower boundary of the stratosphere from measured O_3 mixing ratios. For example, fixed

125 threshold values of typically 70 ppbv or 100 ppbv have been used (e.g., Bethan et al., 1996; Staehelin, 2003). This method has the disadvantage to neglect the seasonal cycle of O_3 and thus the threshold value can be too low or too high when periods exceeding one month are analyzed. Another way to determine the O_3-based tropopause is to take the seasonal cycle into account by using a daily threshold for the O_3 tropopause. This method is described in Zahn et al. (2004) and Thouret et al. (2005) on the basis of long-term observations. In our study we use the method of Zahn et al. (2004) to calculate daily O_3 thresholds for

130 the tropopause. Figure 2 shows the seasonal cycle of the O_3 mixing ratio at the chemical tropopause and the 2 PVU (potential vorticity units, $10^{-6} m^2 s^{-1} K kg^{-1}$) dynamical tropopause, both calculated after Zahn et al. (2004). For the period of our study (16 May to 09 June), we only see small differences in the results between the chemical and the dynamical tropopause since both thresholds are close together around 120 ppbv O_3 during the time of our measurements. We extracted all stratospheric

data (i.e. all data points with O_3 mixing ratios larger than the daily threshold) and calculated the frequency distribution of

135 the potential vorticity from the ERA5 data set (Fig. 2) to verify that the chemical tropopause inferred from the measured O_3

mixing ratios and the calculated thresholds correspond to the dynamical tropopause. This shows that the vast majority of the

stratospheric data points have PV values larger than 2 PVU. In Fig. 2, we observe two modes in the PV distribution of the

stratospheric data which can be explained by the different stratospheric ages of the sampled air masses. In total, less than 4 %

of the data points have PV values below the 2 PVU threshold. Thus we use the definition of the chemical tropopause based on

140 O_3 mixing ratios after Zahn et al. (2004) in this study.

Besides O_3, there are other trace gases used as indicators of stratospheric air masses, e.g. H_2O or N_2O. Moreover, within lim-
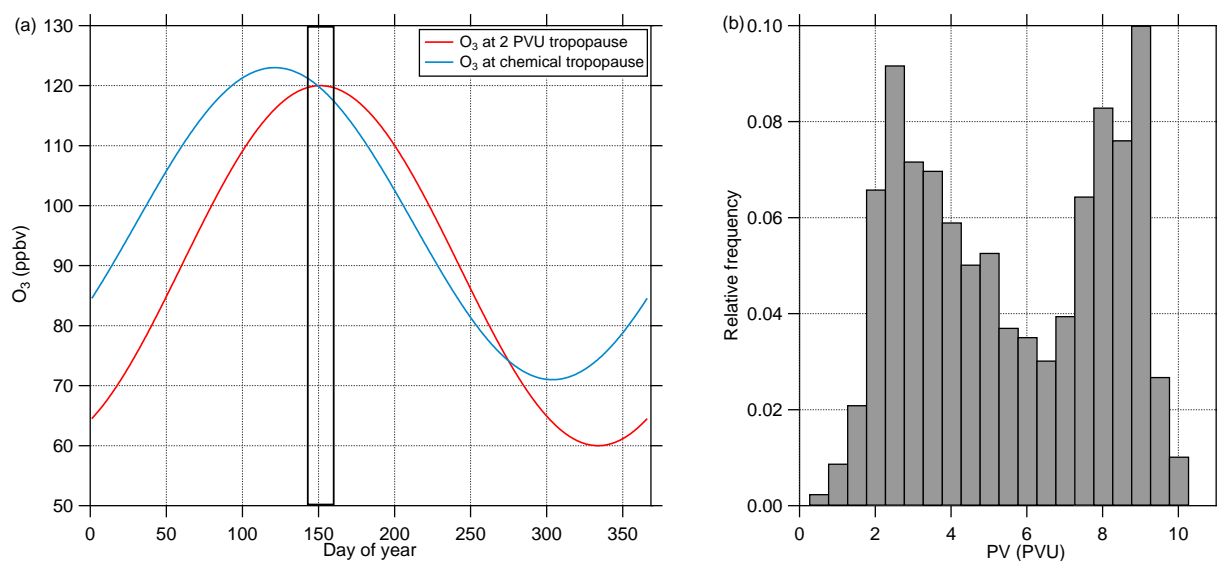
Figure 2. (a) Calculated seasonal cycle of O_3 mixing ratios at the 2 PVU dynamical tropopause and the chemical tropopause, both calculated after Zahn et al. (2004). The measurement period is marked with the solid frame. (b) Relative frequency of PV values the along the AMS data points from CAFE-EU/BLUESKY identified as stratospheric using the calculated O_3 mixing ratios to define the chemical tropopause. Less than 4 % of the data points show PV values lower than 2 PVU indicating a negligible amount of tropospheric air. The complete stratospheric data set holds 2049 data points which represent the 100 % of the subset.

its, aerosol particle properties can be applied as well (Borrmann et al., 1993, 1995). A good example is the mass concentration

of particulate sulfate, which increases in the stratosphere due to the formation from precursors, which takes 30 to 60 days and

reaches its maximum in the Junge layer, where particulate sulfate is present in the form of binary solution droplets with inclu-

145 sions of sulfuric acid (Junge and Manson, 1961; Brühl et al., 2012; Kremser et al., 2016). Thus, we expect a positive correlation

between particulate sulfate and O_3 in the stratosphere. The observations from the CAFE-EU/BLUESKY campaign confirm this

(Fig. 3). Here, two distinct regimes appear in the correlation plot of O_3 and particulate sulfate. In the tropospheric regime, the

sulfate mass concentration shows a high variability at O_3 levels below 100 ppbv, depending on the source regions within the

the boundary layer, e.g. industrial areas. In the stratosphere, we observe a linear correlation between the two species with a

150 slope of 900 to 2300 $\mathrm{ppbv/ppbv}$, but with variations between the individual measurement flights, i.e. on short time scales of

a few days. This analysis shows that the correlation between O_3 and particulate sulfate can be used as a tool for analysing
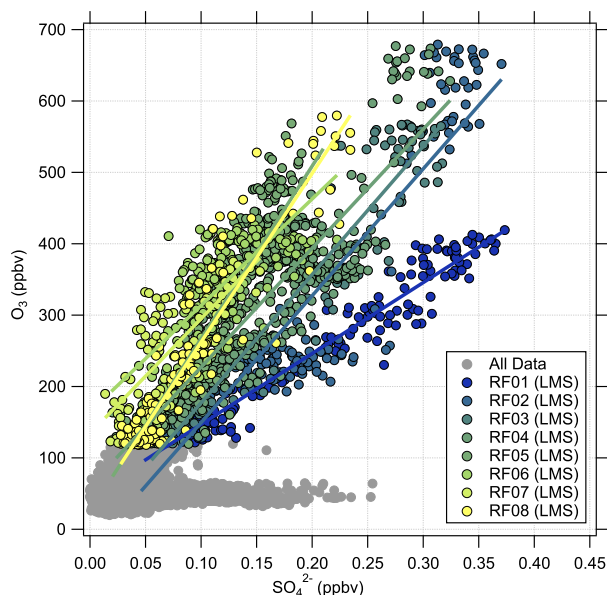
Figure 3. Correlation between O_3 mixing ratio and particulate sulfate mixing ratio for the full CAFE-EU/BLUESKY data set. The color-coded data points indicate the stratospheric data derived from the tropopause O_3 mixing ratios. The grey data shows the complete data set including the tropospheric data. The solid color-coded lines represent the linear regressions for the individual flights.

air masses in terms of their stratospheric character. The variations in the slope and compactness of the correlation appear on

short timescales of a few days. The aim of this study is to understand these variations and link them to possible atmospheric

processes. There are a number of different pathways by which sulfur species can be transported from the troposphere into the

155 stratosphere and thus be a possible reason for the observed variability (e.g., Kremser et al., 2016). Feinberg et al. (2019) show

the modelled atmospheric sulfur budget under volcanically quiescent conditions and the pathways that lead to the formation of

particulate sulfate in the stratosphere. Among these pathways, the most efficient one is the mixing of precursor gases such as

OCS and SO_2 into the stratosphere, where OCS is oxidised to SO_2 and SO_2 is further converted to sulfuric acid, forming sul-

fate aerosol. It is important to emphasise that this budget is valid for volcanically quiescent conditions, because in the presence

160 of volcanic eruptions an additional large source of SO_2 adds up to the other pathways. In this case, SO_2 is transported in the

eruption column up into the free troposphere or even the UTLS region; depending on the strength of the eruption. Then SO_2 is

converted to sulfuric acid and particulate sulfate also in the upper troposphere (Kremser et al., 2016).

Figure 3 shows that direct mixing of sulfate aerosol was not observed during the campaign, due to the low sulfate mixing ratios

at the chemical tropopause, so some other processes need to be taken into account. Previous studies with focus on the Raikoke

165 eruption in 2019 determined no significant contribution from this volcanic eruption (Tomsche et al., 2022; Reifenberg et al.,
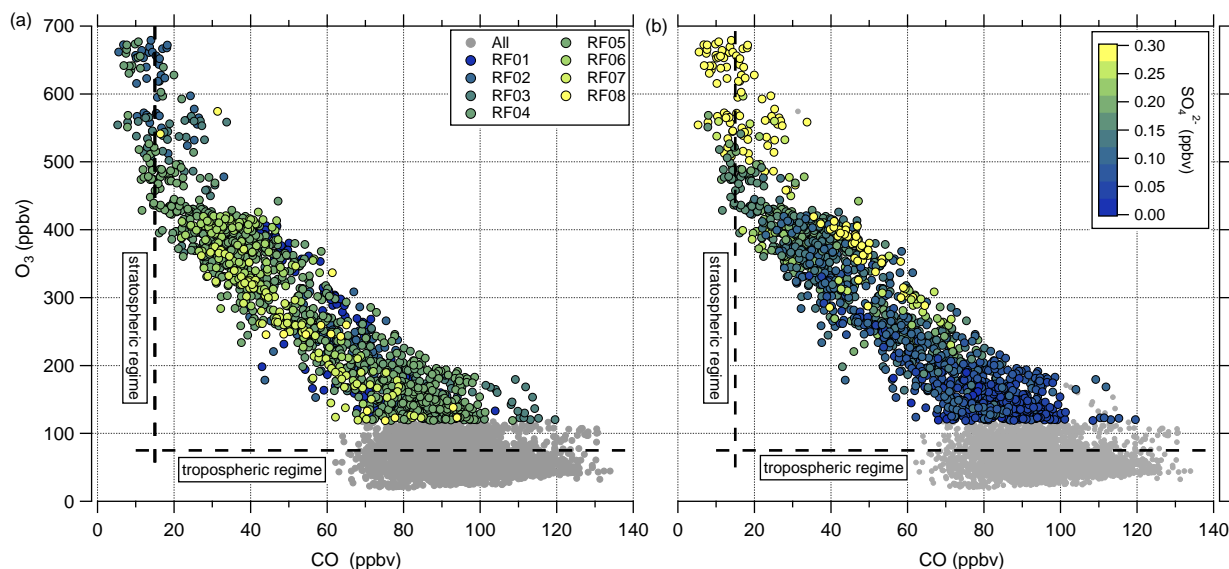
Figure 4. (a) CO-O_3 correlation for all data points in grey and the stratospheric data color-coded with the flight numbers. (b) The same correlation but the stratospheric data is color-coded with the sulfate aerosol mixing ratio. In addition, the dashed lines indicate the mean tropospheric and stratospheric regimes without mixing processes.

2022). The following section will show the influence of cross-tropopause mixing, especially of the precursor gas SO_2 and the potential influence of a more current volcanic eruption.

3.2 Part 2: Case study on aerosol chemical composition related to mixing processes

Volcanic influence is one of the possibilities that can explain the observed variability in the correlation. One major eruption
170 occurred in 2019 by the Raikoke volcano. However, Tomsche et al. (2022) and Reifenberg et al. (2022) showed that this erup-
tion does not have a significant impact on the measurements during CAFE-EU/BLUESKY. In the following, we focus on a
case study to explain the variability, especially for research flight RF01, as the slope in the O_3-SO_4^{2-} correlation for this flight
clearly differs from the other flights (see Fig. 3).

The correlation between CO and O_3 can be used to identify mixing processes between the troposphere and stratosphere (Fis-
175 cher et al., 2000; Hoor et al., 2002). The presence of mixing lines connecting the sampled tropospheric and the stratospheric air
masses indicates recent mixing processes. In Fig. 4, most of the stratospheric data of the whole campaign data set lie on such
mixing lines. Thus, it can be concluded that the measured air masses in the stratosphere are influenced by tropospheric air that
was mixed across the tropopause. As expected, the correlation in Fig. 4b shows much higher particulate sulfate mixing ratios
at higher O_3 levels in the stratosphere and lower mixing ratios close to the tropopause. However, we can identify an anomaly
180 of high particulate sulfate mixing ratios (yellow points) at about 400 ppbv O_3 and 40 ppbv CO (see also Fig. C1). Here, the
measured mixing ratios of sulfate aerosol are in the range we would expect higher up in the stratosphere.

In the following, we will analyze whether this anomaly is caused by a cross-tropopause mixing event and if such events can explain the observed variability in the SO_4-O_3 correlation. For this analysis, we binned our data set along equivalent latitude, which can be used as a dynamical tracer (Butchart and Remsberg, 1986; Hegglin, 2005), and potential temperature to see where the anomaly is located (see Fig. 5). The observed sulfate anomaly occurs in Fig. 5b between 40° N and 45° N at potential temperatures between 345 K and 350 K and is not connected to the stratosphere. The slope of the potential vorticity contour lines indicates that this region is in the vicinity of the jet stream. The sulfate anomaly can not be identified in the O_3 distribution (Fig. 5a), but we can observe the expected increase from the troposphere to the stratosphere. This location of the anomaly is in good agreement with the previous observation that the anomaly is located on a mixing line in the CO-O_3 correlation in a transition regime between the troposphere and the stratosphere.

We further investigate the meteorology over the campaign period to determine whether the anomaly is induced by mixing processes. In particular, we use the vertical wind shear S^2 and the static stability N^2 (see also Appendix B) to identify regions with higher potential for mixing processes. Kaluza et al. (2021) showed in their study that in regions with high vertical wind shear ($S^2 > 4 \cdot 10^{-4}$ s^{-2}), conditions are favourable for rapid mixing. Figure 6 shows the analysis of the stability parameters mentioned above along with the resulting gradient Richardson number. The vertical wind shear shows high values in the region of the sulfate anomaly (see Fig. 6b), exceeding the mentioned threshold for enhanced mixing. This also results in a reduction of the gradient Richardson number in the same bin to values around 1 (see Fig. 6c), which indicates favourable conditions for turbulence. The static stability shows the expected transition from tropospheric to stratospheric values (see Fig. 6a). These findings suggest that mixing occurred in this region and plays a role in the variation of the SO_4-O_3 correlation. To prove this, we investigated the data in the region of the sulfate anomaly in more detail. Therefore, we extracted the data points that contribute to the anomaly. In total there are 45 data points in the bin between 40 and 50° N and 345 to 350 K. The majority of these points (41 points) was sampled during research flight RF01 in a time span of 20 minutes (see Fig. 3). The flight was conducted on 23 May 2020 over Germany, while the anomaly was measured in an area over Lower Saxony (see also Fig. C1 and Fig. C2). A time series of the measurements from this flight is shown in Fig. 7, while the period of the anomaly is marked with a colored box.

Figure 7 reveals the correlation between CO and particulate sulfate in the lower troposphere, as well as the positive correlation between O_3 and particulate sulfate and the anti-correlation between sulfate and CO in the stratosphere. To identify mixing from the measurements, we use two types of scatterplots. The first is the previously introduced scatterplot using CO and O_3 with different color coding (Fig. 8a-c), the second is the scatterplot with H_2O and O_3 (Hegglin et al., 2009) (see Fig. 8d-f). This figure contains only data measured on 23 May 2020. The H_2O-O_3 method follows the same principle, with high water vapor mixing ratios in the troposphere and a constant stratospheric background value around five ppmv as described in Hegglin et al. (2009). All of these scatterplots show two separate branches of mixing lines. The observed sulfate anomaly is located on the upper branch of the mixing lines.

Regardless of the type of scatterplot, we observe an increase in the particulate sulfate mixing ratio and potential temperature along the mixing line, starting at the tropopause and extending into the stratosphere (Fig. 8). In contrast, we also observe a decrease in the CO mixing ratio. This result is consistent with the assumption that tropospheric air enters the stratosphere
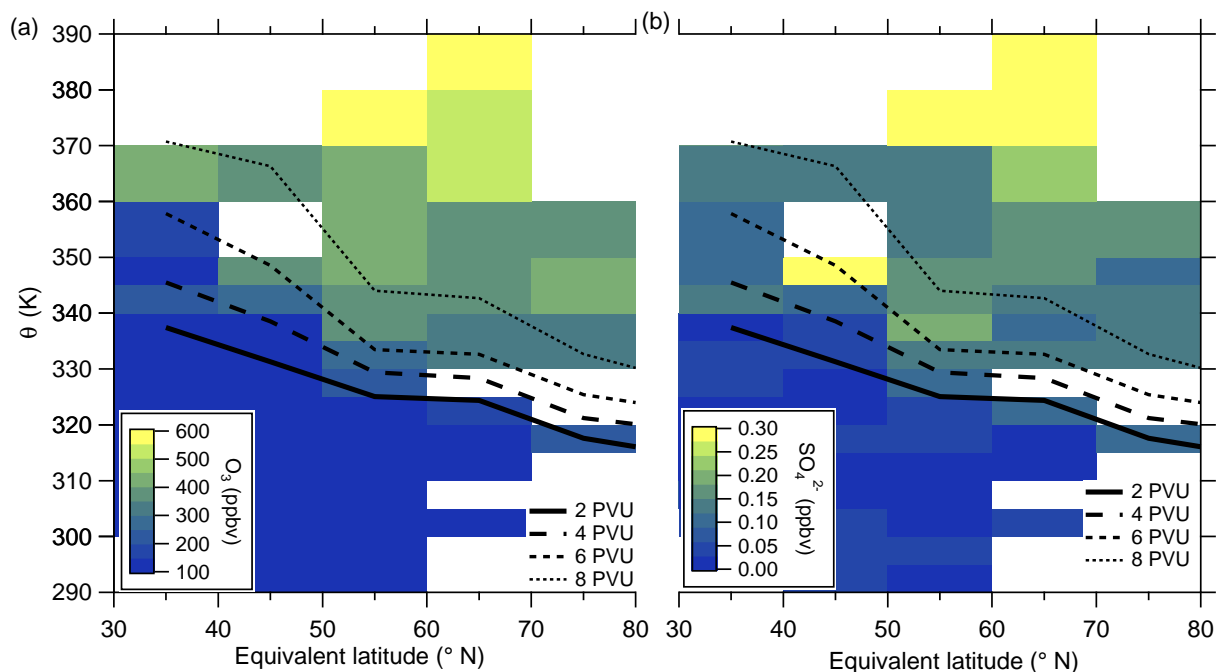
Figure 5. Median of O_3 mixing ratio (a) and sulfate aerosol mixing ratio (b) in the θ-equivalent latitude space. Below 350 K, we use 5 K vertical resolution and $10°$ equivalent latitude bins. Above 350 K, we enlarge the vertical bins to 10 K to obtain a higher statistical evaluation basis (see Fig. A1). In general, only bins with more than 10 data points are evaluated. We added the 2 to 8 PVU lines to show the location of the dynamical tropopause and the extent of the ExTL into the stratosphere. We only show the region of interest for our study between 30 and 80 degrees north.

at lower potential temperatures with lower amounts of sulfate aerosol, accordingly higher mixing ratios of precursor gases, and higher CO. During the slow ascent was consequence of the Brewer-Dobson circulation and the processing of air masses, gas-to-particle conversion of OCS and SO_2 will lead to an increase of particulate sulfate. CO will decrease by dilution and also by photochemical destruction, with an atmospheric lifetime of one to three months (Seinfeld and Pandis, 2016). This is almost the same time as the calculated e-folding time of gas-to-particle conversion of SO_2 to sulfate aerosol in the mid-latitude LMS region (Jurkat et al., 2010).

Further evidence that the anomaly is caused by tropospheric influence are the lower O_3 values and the water vapor mixing ratios. If the air mass were of stratospheric origin, we would expect O_3 mixing ratios higher than 400 ppbv (see Fig. 8) and a water vapor mixing ratio of 10 to 15 ppmv.

Similarly to the HALO measurements, we analysed measurements conducted on the DLR-Falcon for this analysis. The DLR-Falcon performed a measurement flight on the same day and sampled in the area where the anomaly was encountered just 40 min later than HALO (Fig. C2). The DLR-Falcon does not reach the same high altitudes as HALO, so the air masses were probed slightly below and thus show higher CO mixing ratios. This time, we use the scatterplot of CO and HNO_3 to identify
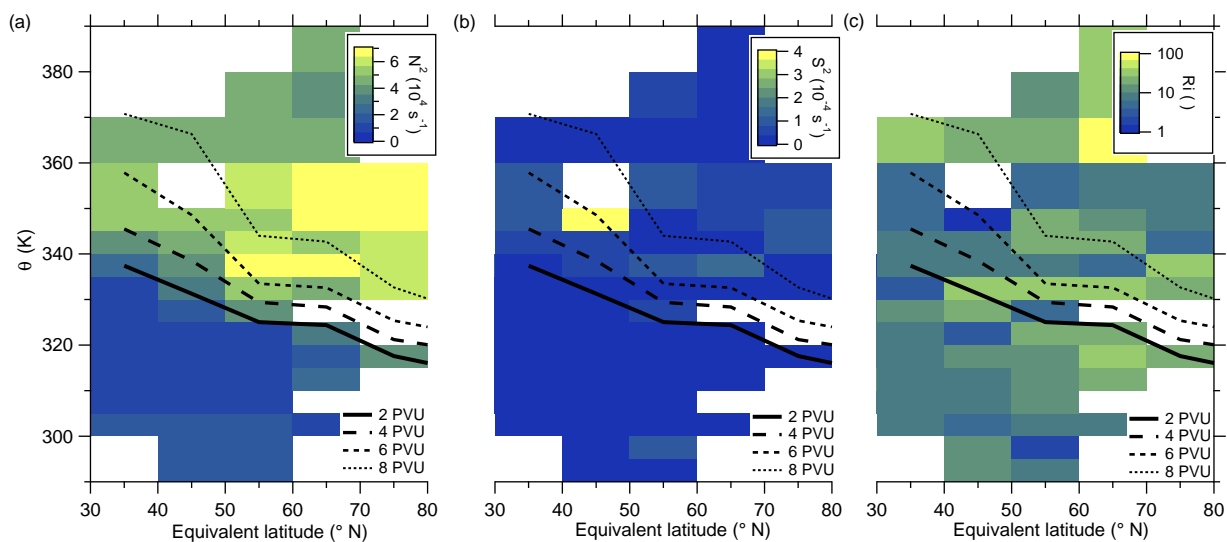
Figure 6. Median of static stability N^2 (a), vertical wind shear S^2 (b) and gradient Richardson number (c) in the θ-equivalent latitude space. Below 350 K, we use 5 K vertical resolution and $10°$ equivalent latitude bins. Above 350 K, we enlarge the vertical bins to 10 K to obtain a higher statistical evaluation basis (see Fig. A1). In general, only bins with more than 10 data points are evaluated. We added the 2 to 8 PVU lines to show the location of the dynamical tropopause and the extent of the ExTL into the stratosphere. We only show the region of interest for our study between 30 and 80 degrees north.

230 mixing in combination with gas-to-particle conversion (Fig. 9). HNO_3 was already introduced as a stratospheric tracer by Proffitt et al. (1989) or Arnold et al. (1989) and utilised because the O_3 data for the DLR-Falcon are not available for this flight. We identify a mixing line in the scatterplot, connecting troposphere and stratosphere. The SO_2 mixing ratios on this mixing line are elevated with respect to the measured stratospheric values around 0.04 ppbv but already reduced from their measured tropospheric maxima of 0.01 ppbv, which is an indication for gas-to-particle conversion along this mixing line.

235 As a complement to the measurement data, we analyzed the meteorological situation along the flight path for the period of the anomaly (Fig. B1). The flight path was located just above the maximum of the subtropical jet stream and a layer of strong vertical wind shear (Fig. B1a). Further, we see that the flight path crossed a layer of low gradient Richardson number (Fig. B1)b, and later continued slightly above this layer. This indicated a region of instability which is an important factor for mixing processes. The preceding discussion has shown that very likely mixing between tropospheric and stratospheric air masses

240 occurred prior to the in-situ measurements.

Hereafter, we examine the origin of the air masses comprised of high mixing ratios of sulfate aerosol. Therefore, we exploit LAGRANTO backward trajectories starting at a grid around the flight path with 230 trajectories for each measurement point. The trajectories are calculated 10 days backward, to see whether the air masses ascended in regions with higher concentrations of precursor gases or even crossed such regions in the upper troposphere. For our analysis, we filtered the trajectories

245 by selecting only those with a minimum potential temperature below 345 K and with an increase of at least 5 K potential
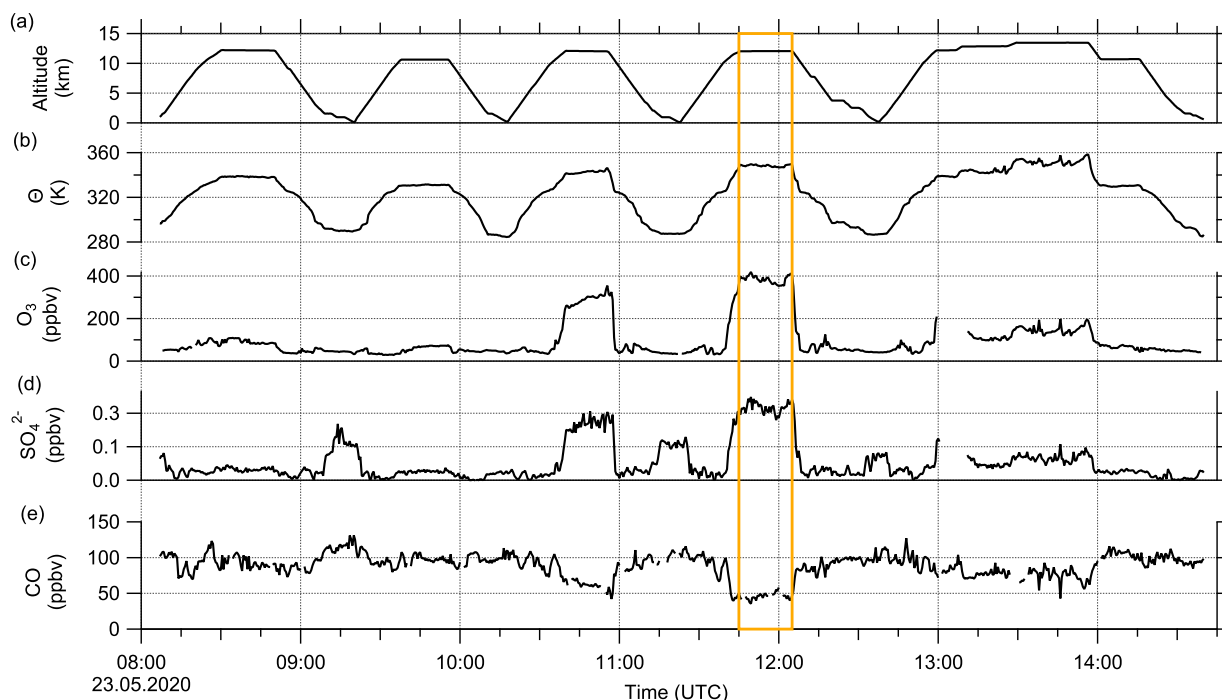
Figure 7. Time series of in-situ measurements during research flight RF01 on 23 May 2020 in 30 s time steps. (a) Altitude, (b) potential temperature θ, (c) O_3 mixing ratios, (d) sulfate aerosol mixing ratios and (e) CO mixing ratios. The orange box marks the period with the observed sulfate anomaly described in the text and shown in Fig. C1.

temperature. Figure 10 shows that the selected trajectories are close together and move with the jet stream. The trajectories cross the region of East Asia within 10 days before the measurement and most of them crossed China and its megacities like Chengdu and Shanghai. The time series of potential temperature shows that no boundary layer air masses were transported to the measurement region in the last 10 days (Fig. 10a), considering the assumption that the trajectories can resolve convective
250 uplift. As a consequence, the enhanced particulate sulfate needs to be older than 10 days and was most likely not directly mixed into the LMS as particulate sulfate.

Alternatively, the sulfate aerosol could originate from gas-to-particle conversion of SO_2 that was mixed into the LMS. To examine this hypothesis, we start from Fig. 9, which shows that close to the tropopause, the SO_2 values are quite high and are decreasing along the mixing line. This is an indicator for ongoing gas-to-particle conversion in combination with cross-
255 tropopause mixing. A possible source for the high SO_2 mixing ratios in the troposphere and close to the tropopause could be volcanic activities. Therefore, we searched for volcanic eruptions in the period of two months before the measurements, corresponding to the e-folding time of about 50 to 60 days (Jurkat et al., 2010). For the analysis, we used daily TROPOMI retrievals in different volcanically active regions to identify possible source regions. Thereby, we identified the Kamchatka Peninsula in Russia as an origin of enhanced SO_2 emissions in the beginning of April 2020. This corresponds to the archived reports by the
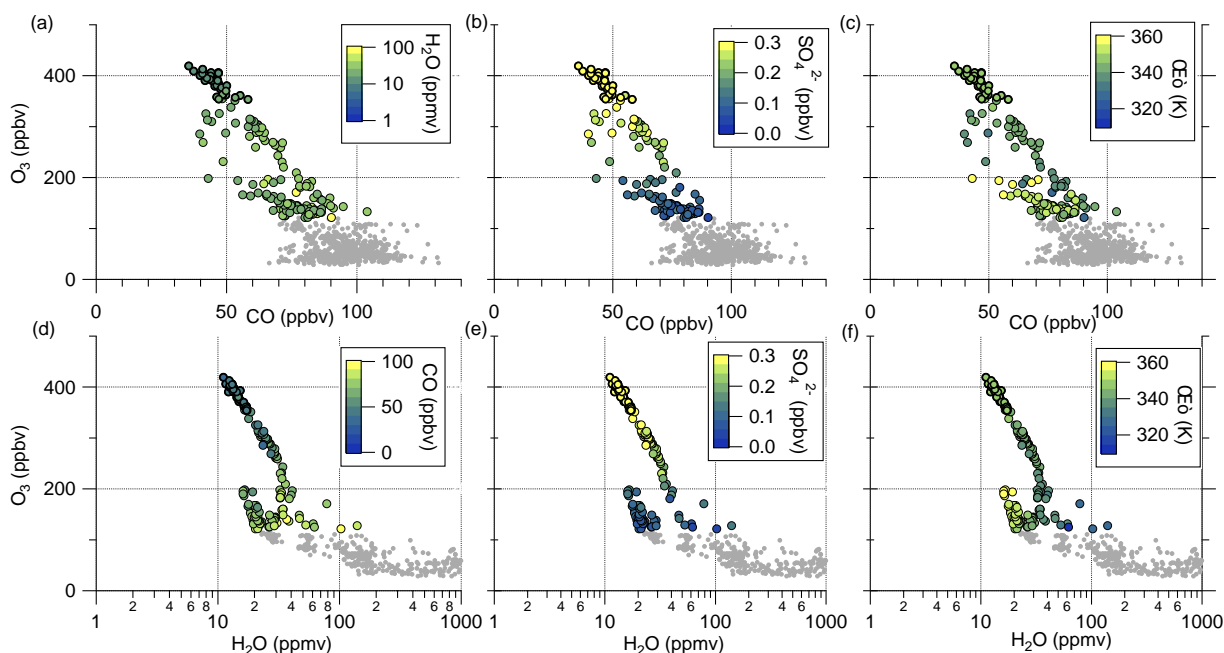
Figure 8. Tracer-tracer correlations for 23 May 2020 to identify mixing processes. The CO-O_3 correlations are color-coded with (a) SO_4^{2-}, (b) θ and (c) H_2O. The H_2O-O_3 correlations are color-coded with (d) SO_4^{2-}, (e) θ and (f) CO. The data correspond to the blue colored data in Fig. 3 and the sulfur anomaly in Fig. 5.

Kamchatka Volcanic Eruption Response Team (KVERT) (Institute of Volcanology and Seismology FEB RAS, 2023). In the report for 08 April 2020, an explosive eruption of the Sheveluch volcano is described, with a volcanic cloud height reaching up to 10 km and thus into the tropopause region. We performed HYSPLIT (Stein et al., 2015) forward dispersion simulations of the Sheveluch volcano plume and analyzed the eruption plume in the model in different heights to get a broad overview of the distribution. Therefore, we calculated forward trajectories in heights between 9000 and 11000 m with a vertical resolution of 500 m. In the following, we only consider the levels up to 9000 m (see Fig. D1) and between 10000 and 11000 m (see Fig. 11), because here the model shows differences in the plume and indicates possible mixing into the stratosphere. We observe a large volcanic plume up to 9000 m which is distributed, spread and stretched within the first three days over the Northern Pacific reaching over Alaska and also eastwards, close to the Hudson Bay, Canada (see Fig. D1). For the layer between 10000 and 11000 m, the results look completely different (see Fig. 11). Here, we observe no signal of the volcanic plume on the first day. However, more areas with volcanic plume influence occur over Alaska reaching towards Canada during the second day. These affected areas increase over time. Thus, also the HYSPLIT dispersion model results support the hypothesis of mixing volcanic emissions into the stratosphere within the first three days. This is an additional indicator for the mixing of SO_2 into the stratosphere, resulting in higher SO_2 mixing ratios compared to the background. After the mixing of SO_2 into the LMS, the process of gas-to-particle conversion starts and forms particulate sulfate aerosol over several weeks. This results in the
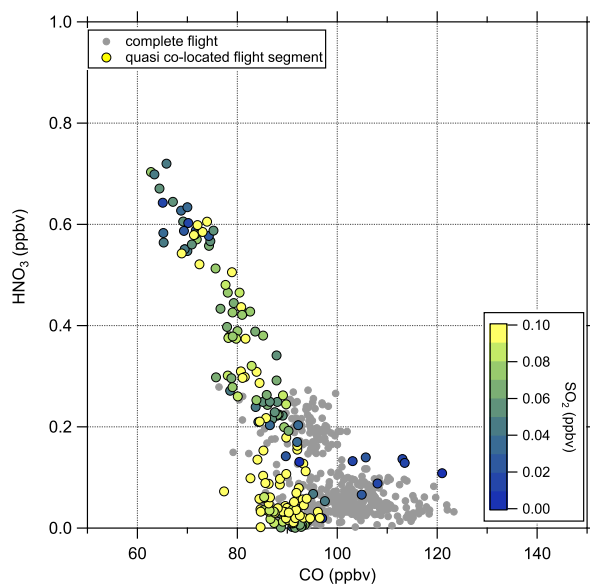
Figure 9. Scatterplot of CO and HNO₃ for the DLR-Falcon flight on 23 May 2020. The quasi co-located measurements with HALO are color-coded with SO2. Here, a mixing event was observed in the HALO data. The DLR-Falcon did not reach the high altitudes of HALO, so the lowest CO values are higher.
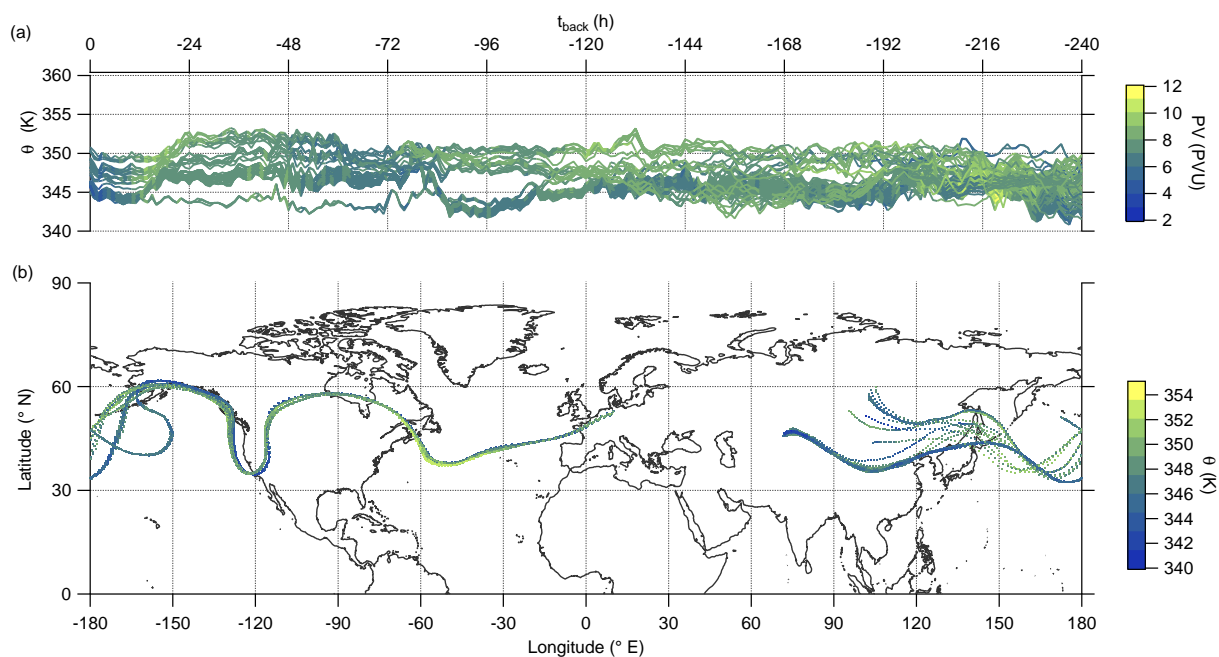
Figure 10. LAGRANTO 10 days back trajectories for cases with enhanced SO_4^{2-} in the lowermost stratosphere. The upper panel (a) shows a time series of θ color-coded with PV. The lower panel (b) shows the position of the trajectories on the map and θ as color-code.
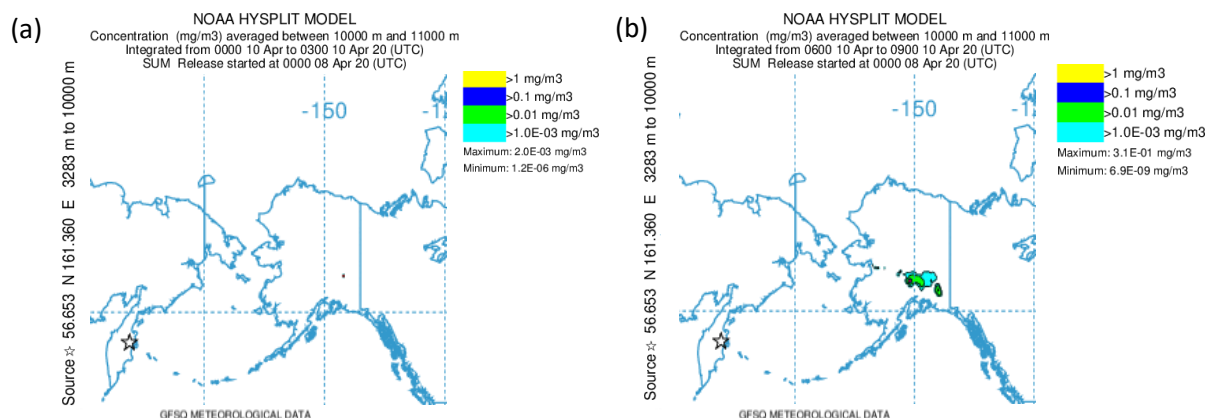
Figure 11. NOAA HYSPLIT dispersion model simulation (Stein et al., 2015) for the Sheveluch eruption on 08 April 2020 on basis of GFS meteorological data. The particle concentration between 10000 and 11000 m is depicted. (a) shows the averaging period on 10 April 2020 from 00 UTC until 03 UTC and (b) shows the next period on 10 April 2020 from 06 UTC until 09 UTC.

275 observation of higher mixing ratios of particulate sulfate in the LMS roughly seven weeks after the eruption, especially for research flight RF01 where the flight path was close to the jet stream and crossed one filament of volcanically influenced air masses.

4 Conclusions

Usually trace gas correlations, such as O_3-CO or O_3-H_2O, have been used to study mixing processes between the troposphere
280 and stratosphere. In our study, we showed that in addition to trace gas measurements, also aerosol measurements, especially particulate sulfate, can be applied to identify troposphere-stratosphere exchange. Furthermore, we showed that the method to define the chemical tropopause proposed by Zahn et al. (2004) is in agreement with the dynamical tropopause definition for our campaign and thus suitable for the separation of stratospheric and tropospheric air masses. Similar to the correlation between CO and O_3, the correlation of SO_4^{2-} and O_3 in the lowermost stratosphere also showed some variability induced by
285 mixing events. In a case study during the CAFE-EU/BLUESKY mission, we observed air masses with high sulfate mixing ratios in the lowermost stratosphere, reaching values that are typically found at higher altitudes in the stratospheric aerosol layer. Meteorological and dynamical parameters such as vertical wind shear and gradient Richardson number indicated that mixing across the tropopause occurred in this region and along the transport and air mass history. Additionally, we found that this anomaly of higher particulate sulfate in the lowermost stratosphere occurred during one single flight. During this flight, we
290 found one single mixing line in the CO-O_3 correlation with increasing sulfate aerosol mixing ratios towards the stratosphere. In addition, we used measurements of the quasi co-located DLR-Falcon aircraft. In the same tracer-tracer correlation framework, using HNO_3 instead of O_3, we also found one mixing line. In contrast to the increasing sulfate for the HALO measurements, we observed decreasing mixing ratios of SO_2 which is a precursor gas for particulate sulfate. This led to the hypothesis of upward

mixing of precursor gases and on-going gas-to-particle conversion in the lowermost stratosphere. Here, we could identify
volcanic activities on the Kamchatka Peninsula, Russia, and the explosive eruption of the Sheveluch volcano as a possible
source for the SO$_2$. The Sheveluch eruption injected SO$_2$ directly into the upper troposphere from where it was mixed into the
stratosphere, with subsequent gas-to-particle conversion to sulfate aerosol. We can thus conclude that the chemical composition
of the aerosol in the lowermost stratosphere is affected by small-scale mixing processes, and that the ExTL can thus also be
characterized by aerosol properties. In addition to direct mixing of aerosol particles, the process of mixing of precursor gases
with subsequent gas-to-particle conversion needs also to be considered, as we showed in our case study. We intend to use this
method in the future with data obtained during previous airborne measurements in the UTLS to extend the analysis to a larger
scale. Furthermore, we aim to compare the results with chemistry climate model studies to see whether chemical transport
models can represent small-scale mixing across the tropopause and the associated gas-to-particle conversion processes. Another
study should investigate how models represent the influence of volcanic eruptions on the lowermost stratosphere.

Data availability. Data measured onboard HALO are available on request at the HALO database at https://halo-db.pa.op.dlr.de/mission/120.
The DLR-Falcon basic aircraft data and the AIMS data are available on request at the HALO database at https://halo-db.pa.op.dlr.de/mission/
119 (Re3data.Org, 2016) or on request to the authors.

Author contributions. PJ set up the study together with JS, performed the data analysis and prepared the manuscript. KK and JS provided
the sulfate data and supported the analysis. LT, AM and CV provided the SO$_2$ and HNO$_3$ data. HS provided CO and O$_3$ data from DLR-
Falcon. AZ provided the O$_3$ data from HALO. HF and LR provided CO data from HALO. HCL and DK provided model data and backward
trajectories as well as the code for the cross sections along the flight path. All co-authors commented on the manuscript and discussed the
presented results.

Competing interests. The contact author has declared that none of the authors has any competing interests.

Acknowledgements. PJ is funded by the Deutsche Forschungsgemeinschaft (DFG, German Research Foundation) – TRR 301 – Project-ID
428312742: "The tropopause region in a changing atmosphere", sub-project A04 coordinated by J. Schneider, S. Borrmann and F. Köll-
ner. LT and CV are funded as well by the TRR 301 – Project-ID 428312742 in sub-project A01. The HALO measurement flights during
CAFE-EU/BLUESKY were funded by the Max Planck Society. The authors thank the DLR team for making a campaign possible during the
COVID-19 lockdown in Germany.
The authors thank NOAA Air Resources Laboratory for providing the HYSPLIT dispersion calculations on their website.

Appendix A: Supporting information about the 2-D binned cross sections

In the following, we explain the adjustment of our bin scheme for the two dimensional binning analysis. Figure A1b shows the data distribution for the evenly distributed bin scheme in the vertical. Here, we see that many bins in the LMS contain less than 10 data points, so we could expect some bias in the median. Therefore, we enlarge the vertical bins at 350 K and above to 10 K to include more data points in one vertical bin and increase the statistic of the analysis without losing information.
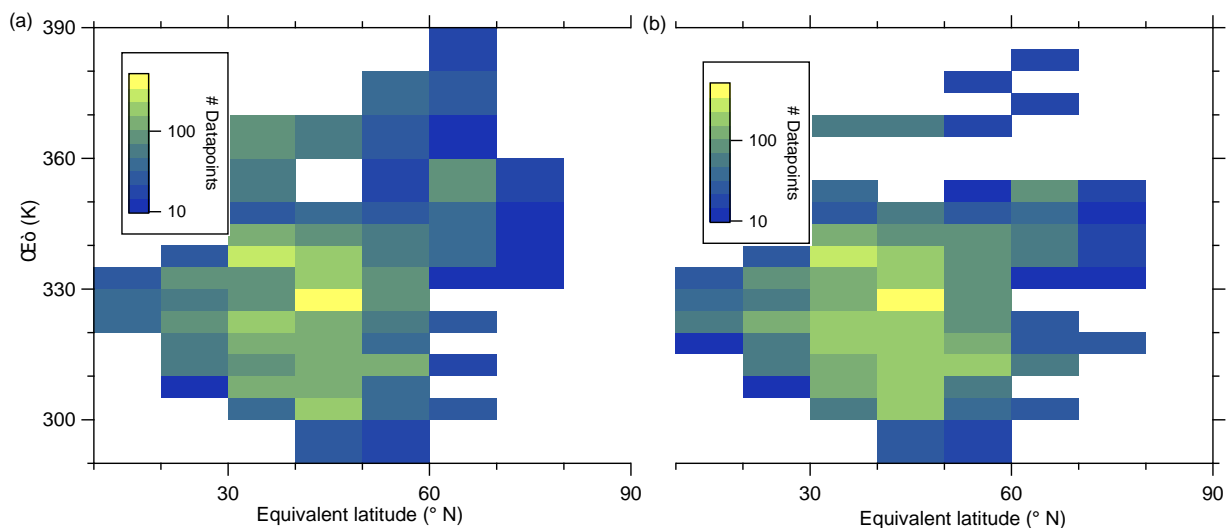
Figure A1. Number of data points in the 2-D cross sections (used in Fig. 5 and Fig. 6). (a) The used bin scheme with larger vertical bins starting at $\theta > 350$ K. (b) The evenly data distribution without any adjustment on the bin scheme.

325

Appendix B: Supporting information about the meteorological cross sections

This section offers some meteorological analysis for the flight segment with the observed particulate sulfate anomaly (see Fig. B1). Afterwards, we show some additional data along the back trajectories. More precisely, we show the time series of the Richardson number to indicate potential instable regions the air masses have crossed before the measurement (see Fig. B2).

330   First we want to introduce the used variables for our stability analysis, similar to e.g., Kaluza et al. (2019) or Kunkel et al. (2019):

$$N^2 = -\frac{g}{\rho_0}\frac{\partial \rho(z)}{\partial z} \quad \text{squared Brunt–Väisälä frequency} \tag{B1}$$

$$S^2 = (\frac{\partial u}{\partial z})^2 + (\frac{\partial v}{\partial z})^2 \quad \text{vertical wind shear} \tag{B2}$$

$$Ri = \frac{N^2}{S^2} \quad \text{gradient Richardson number} \tag{B3}$$

335   Turbulence may occur at a gradient Richardson number lower than 0.25
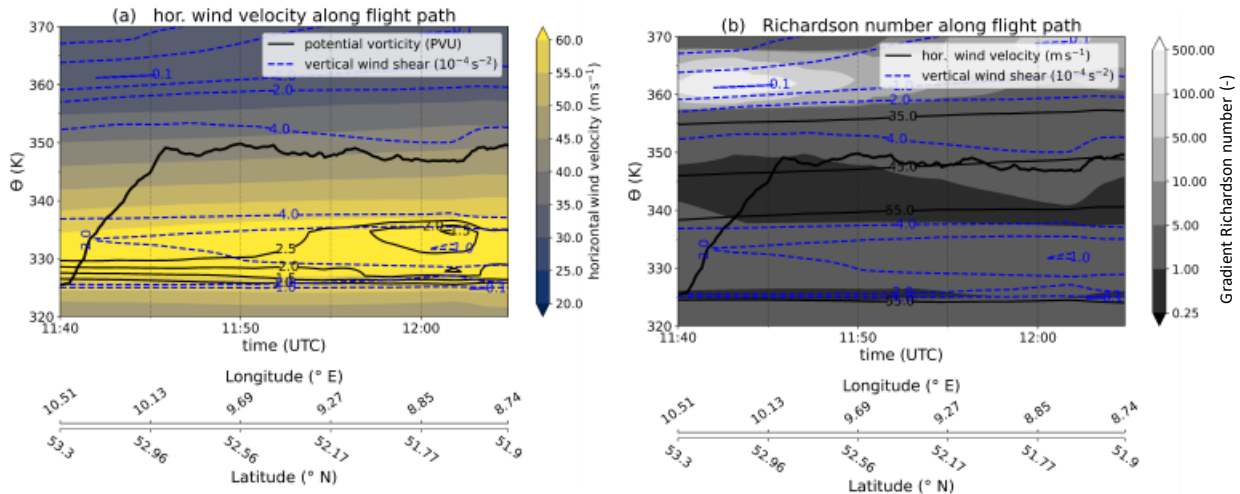
Figure B1. Meteorological cross sections along the flight path, calculated on the basis of ERA5-reanalysis data (Hersbach et al., 2020). (a) contains the horizontal wind speed as filled contour, the flight altitude as black bold solid line, the PV contour as thin black lines and the vertical wind shear as dashed blue contour lines. In (b) the filled contour changed to the gradient Richardson number and the thin black lines are contour lines of the horizontal wind speed. Latitude and longitude values are added to the time series for reference.
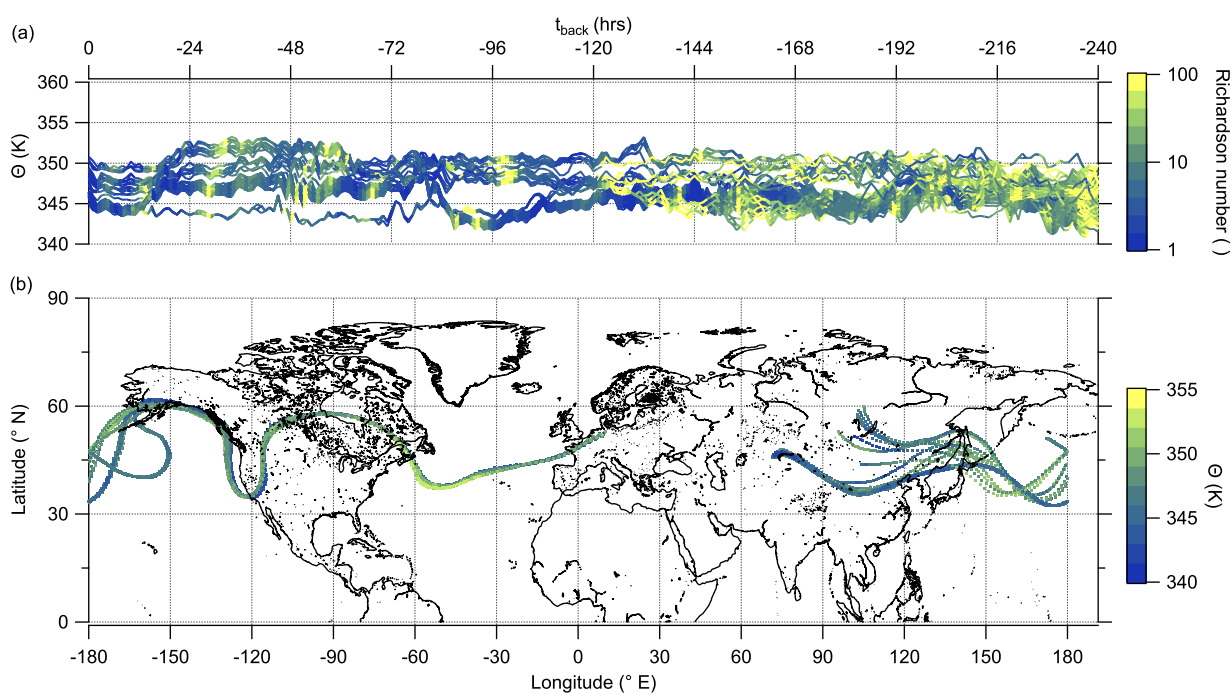
Figure B2. LAGRANTO 10 days back trajectories for cases with enhanced SO_4^{2-} in the lowermost stratosphere starting in Northern Germany. (a) Time series of θ color-coded with the gradient Richardson number as marker for potentially instable regions along the trajectories. (b) The position of the trajectories on the map and the potential temperature as color-code.

Appendix C: Supporting information about the sulfate anomaly

The following figures are supporting information on the observed anomaly of higher mixing ratios of particulate sulfate. This includes a detailed view on the research flight RF01 where the anomaly was observed (Fig. C1). Figure C2 locates the flight segment of the anomaly on the map including the quasi co-located DLR-Falcon flight path and the sulfur dioxide mixing ratio measured on the DLR-Falcon. The last figure (Fig. C3) highlights two selected research flights and their corresponding accuracy within the correlation of the complete data set.
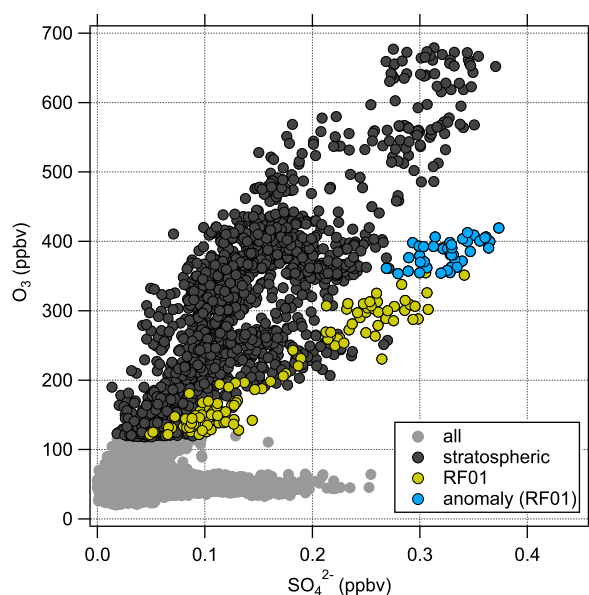
Figure C1. Scatter plot of the in-situ measured SO_4^{2-} and O_3 containing/including the whole campaign data in bright grey. Stratospheric data points are colored in dark grey. The mixing event of research flight RF01 is indicated in yellow and the sulfate anomaly identified during this flight in blue.
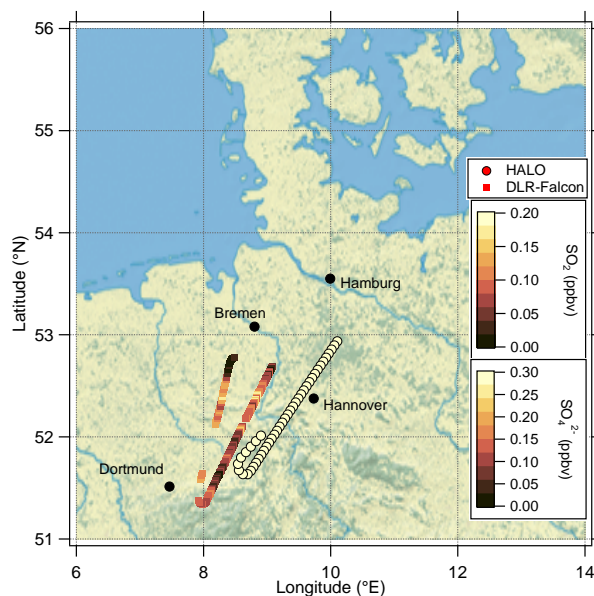
Figure C2. Location of the analyzed flight segment during the research flight on 23 May 2020 between 11:45 and 12:05 UTC where the mixing event in the vicinity of the jetstream was observed. The flight path of HALO are the filled circles with color-coded with the sulfate mixing ratio and the flight path of DLR-Falcon are the filled squares color-coded with the SO_2 mixing ratio. The map was created from public domain GIS data found on the Natural Earth website (http://www.naturalearthdata.com; last access: 02 January 2024)
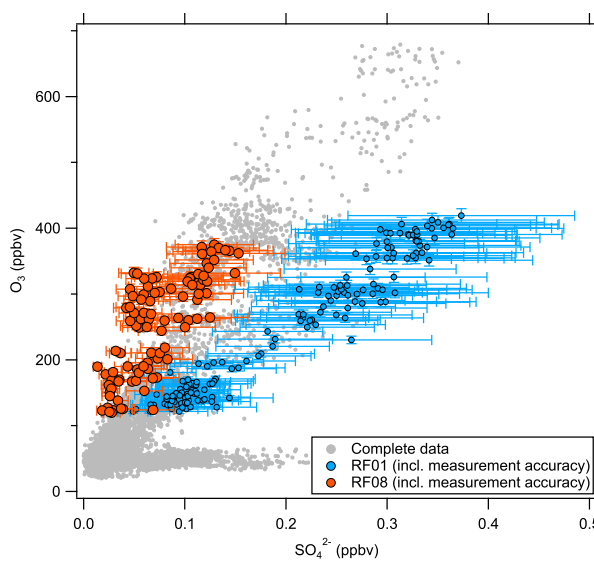
Figure C3. Scatterplot of particulate sulfate against O_3 for the complete campaign data set. The data points for flights RF01 and RF08 are highlighted together with their measurement accuracy as examples.

Appendix D: Supporting information about the HYSPLIT dispersion simulation

The figure shown in this section is in addition to Fig. 11 and shows the similar variables but for the altitude range from sea level up to 9000 m to show the entire volcanic main plume and its distribution.
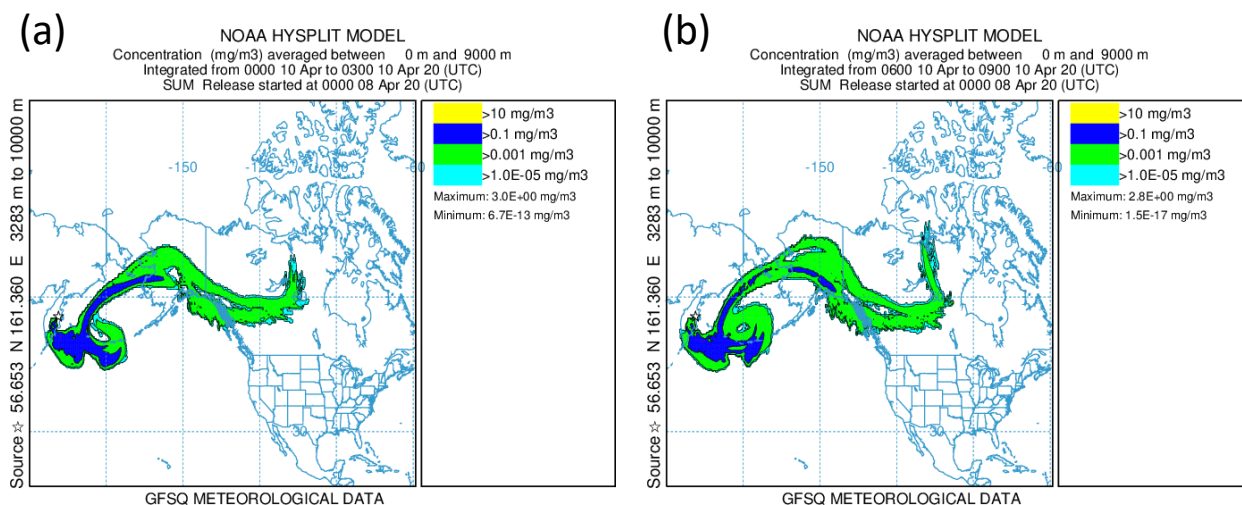
Figure D1. NOAA HYSPLIT dispersion model simulation for the Sheveluch eruption on 08 April 2020 on basis of GFS meteorological data (Stein et al., 2015). The location of Sheveluch volcano is given by a little star. Further, the particle concentration averaged between sea level and 9000 m is shown. (a) includes the averaging period on 10 April 2020 from 00 UTC to 03 UTC and (b) shows the next period on the same day from 06 UTC to 09 UTC.

References

Andreae, M. O.: Ocean-atmosphere interactions in the global biogeochemical sulfur cycle, Marine Chemistry, 30, 1–29, https://doi.org/10.1016/0304-4203(90)90059-l, 1990.

Appel, O., Köllner, F., Dragoneas, A., Hünig, A., Molleker, S., Schlager, H., Mahnke, C., Weigel, R., Port, M., Schulz, C., Drewnick, F., Vogel, B., Stroh, F., and Borrmann, S.: Chemical analysis of the Asian tropopause aerosol layer (ATAL) with emphasis on secondary aerosol particles using aircraft-based in situ aerosol mass spectrometry, Atmospheric Chemistry and Physics, 22, 13 607–13 630, https://doi.org/10.5194/acp-22-13607-2022, 2022.

Arnold, F., Schlager, H., Hoffmann, J., Metzinger, P., and Spreng, S.: Evidence for stratospheric nitric acid condensation from balloon and rocket measurements in the Arctic, Nature, 342, 493–497, 1989.

Barré, J., Amraoui, L. E., Ricaud, P., Lahoz, W. A., Attié, J.-L., Peuch, V.-H., Josse, B., and Marécal, V.: Diagnosing the transition layer at extratropical latitudes using MLS O&ltsub&gt3&lt/sub&gt and MOPITT CO analyses, Atmospheric Chemistry and Physics, 13, 7225–7240, https://doi.org/10.5194/acp-13-7225-2013, 2013.

Bethan, S., Vaughan, G., and Reid, S. J.: A comparison of ozone and thermal tropopause heights and the impact of tropopause definition on quantifying the ozone content of the troposphere, Quarterly Journal of the Royal Meteorological Society, 122, 929–944, https://doi.org/10.1002/qj.49712253207, 1996.

Borrmann, S., Dye, J. E., Baumgardner, D., Wilson, J. C., Jonsson, H. H., Brock, C. A., Loewenstein, M., Podolske, J. R., Ferry, G. V., and Barr, K. S.: In-situ measurements of changes in stratospheric aerosol and the Nsub2/subO-aerosol relationship inside and outside of the polar vortex, Geophysical Research Letters, 20, 2559–2562, https://doi.org/10.1029/93gl01694, 1993.

Borrmann, S., Dye, J. E., Baumgardner, D., Proffitt, M. H., Margitan, J. J., Wilson, J. C., Jonsson, H. H., Brock, C. A., Loewenstein, M., Podolske, J. R., and Ferry, G. V.: Aerosols as dynamical tracers in the lower stratosphere: Ozone versus aerosol correlation after the Mount Pinatubo eruption, Journal of Geophysical Research: Atmospheres, 100, 11 147–11 156, https://doi.org/10.1029/95jd00016, 1995.

Brimblecombe, P.: The Global Sulfur Cycle, p. 559–591, Elsevier, https://doi.org/10.1016/b978-0-08-095975-7.00814-7, 2014.

Brühl, C., Lelieveld, J., Crutzen, P. J., and Tost, H.: The role of carbonyl sulphide as a source of stratospheric sulphate aerosol and its impact on climate, Atmospheric Chemistry and Physics, 12, 1239–1253, https://doi.org/10.5194/acp-12-1239-2012, 2012.

Butchart, N. and Remsberg, E. E.: The Area of the Stratospheric Polar Vortex as a Diagnostic for Tracer Transport on an Isentropic Surface, Journal of the Atmospheric Sciences, 43, 1319–1339, https://doi.org/10.1175/1520-0469(1986)043<1319:taotsp>2.0.co;2, 1986.

Canagaratna, M. R., Canagaratna, M. R., Jayne, J. T., Jimenez, J. L., Allan, J., Alfarra, M. R., Alfarra, M. R., Zhang, Q., Zhang, Q., Zhang, Q., Onasch, T. B., Onasch, T. B., Drewnick, F., Coe, H., Middlebrook, A. M., Delia, A. E., Williams, L. R., Trimborn, A., Northway, M. J., Northway, M. J., DeCarlo, P. F., Kolb, C. E., Davidovits, P., and Worsnop, D. R.: Chemical and microphysical characterization of ambient aerosols with the aerodyne aerosol mass spectrometer, Mass Spectrometry Reviews, https://doi.org/10.1002/mas.20115, 2007.

Crutzen, P. J.: The possible importance of CSO for the sulfate layer of the stratosphere, Geophysical Research Letters, 3, 73–76, https://doi.org/10.1029/GL003i002p00073, 1976.

Deshler, T.: A review of global stratospheric aerosol: Measurements, importance, life cycle, and local stratospheric aerosol, Atmospheric Research, 90, 223–232, https://doi.org/10.1016/j.atmosres.2008.03.016, 2008.

Drewnick, F., Hings, S. S., DeCarlo, P. F., Jayne, J. T., Gonin, M., Fuhrer, K., Weimer, S., Jimenez, J. L., Demerjian, K. L., Borrmann, S., Borrmann, S., and Worsnop, D. R.: A New Time-of-Flight Aerosol Mass Spectrometer (TOF-AMS)—Instrument Description and First Field Deployment, Aerosol Science and Technology, https://doi.org/10.1080/02786820500182040, 2005.

Fadnavis, S., Semeniuk, K., Pozzoli, L., Schultz, M. G., Ghude, S. D., Das, S., and Kakatkar, R.: Transport of aerosols into the UTLS and their impact on the Asian monsoon region as seen in a global model simulation, Atmospheric Chemistry and Physics, 13, 8771–8786, https://doi.org/10.5194/acp-13-8771-2013, 2013.

385   Feinberg, A., Sukhodolov, T., Luo, B., Luo, B., Rozanov, E., Winkel, L. H. E., Peter, T., and Stenke, A.: Improved tropospheric and stratospheric sulfur cycle in the aerosol-chemistry-climate model SOCOL-AERv2, Geoscientific Model Development, https://doi.org/10.5194/gmd-12-3863-2019, 2019.

Fischer, H., Wienhold, F. G., Hoor, P., Bujok, O., Schiller, C., Siegmund, P., Ambaum, M., Scheeren, H. A., and Lelieveld, J.: Tracer correlations in the northern high latitude lowermost stratosphere: Influence of cross-tropopause mass exchange, Geophysical Research

390   Letters, 27, 97–100, https://doi.org/10.1029/1999GL010879, 2000.

Friberg, J., Martinsson, B. G., Andersson, S. M., Brenninkmeijer, C. A. M., Hermann, M., Van Velthoven, P. f. J., and Zahn, A.: Sources of increase in lowermost stratospheric sulphurous and carbonaceous aerosol background concentrations during 1999–2008 derived from CARIBIC flights, Tellus B: Chemical and Physical Meteorology, 66, 23 428, https://doi.org/10.3402/tellusb.v66.23428, 2014.

Friberg, J., Martinsson, B. G., Andersson, S. M., and Sandvik, O. S.: Volcanic impact on the climate – the stratospheric aerosol load in the

395   period 2006–2015, Atmospheric Chemistry and Physics, 18, 11 149–11 169, https://doi.org/10.5194/acp-18-11149-2018, 2018.

Froyd, K. D., Murphy, D. M., Sanford, T. J., Thomson, D. S., Wilson, J. C., Pfister, L., and Lait, L.: Aerosol composition of the tropical upper troposphere, Atmospheric Chemistry and Physics, 9, 4363–4385, https://doi.org/10.5194/acp-9-4363-2009, 2009.

Gettelman, A., Hoor, P., Pan, L. L., Randel, W. J., Hegglin, M. I., and Birner, T.: THE EXTRATROPICAL UPPER TROPOSPHERE AND LOWER STRATOSPHERE, Reviews of Geophysics, 49, RG3003, https://doi.org/10.1029/2011RG000355, 2011.

400   Gorkavyi, N., Krotkov, N., Li, C., Lait, L., Colarco, P., Carn, S., DeLand, M., Newman, P., Schoeberl, M., Taha, G., Torres, O., Vasilkov, A., and Joiner, J.: Tracking aerosols and SO<sub>2</sub> clouds from the Raikoke eruption: 3D view from satellite observations, Atmospheric Measurement Techniques, 14, 7545–7563, https://doi.org/10.5194/amt-14-7545-2021, 2021.

Hegglin, M. I.: Determination of eddy diffusivity in the lowermost stratosphere, Geophysical Research Letters, 32, https://doi.org/10.1029/2005gl022495, 2005.

405   Hegglin, M. I., Boone, C. D., Manney, G. L., and Walker, K. A.: A global view of the extratropical tropopause transition layer from Atmospheric Chemistry Experiment Fourier Transform Spectrometer O 3 , H 2 O, and CO, Journal of Geophysical Research, 114, D00B11, https://doi.org/10.1029/2008JD009984, 2009.

Hersbach, H., Bell, B., Berrisford, P., Hirahara, S., Horányi, A., Muñoz-Sabater, J., Nicolas, J., Peubey, C., Radu, R., Schepers, D., Simmons, A., Soci, C., Abdalla, S., Abellan, X., Balsamo, G., Bechtold, P., Biavati, G., Bidlot, J., Bonavita, M., Chiara, G., Dahlgren, P., Dee,

410   D., Diamantakis, M., Dragani, R., Flemming, J., Forbes, R., Fuentes, M., Geer, A., Haimberger, L., Healy, S., Hogan, R. J., Hólm, E., Janisková, M., Keeley, S., Laloyaux, P., Lopez, P., Lupu, C., Radnoti, G., Rosnay, P., Rozum, I., Vamborg, F., Villaume, S., and Thépaut, J.-N.: The ERA5 global reanalysis, Quarterly Journal of the Royal Meteorological Society, 146, 1999–2049, https://doi.org/10.1002/qj.3803, 2020.

Hofmann, D. J. and Rosen, J. M.: On the Background Stratospheric Aerosol Layer, Journal of the Atmospheric Sciences, 38, 168–181,

415   https://doi.org/10.1175/1520-0469(1981)038<0168:otbsal>2.0.co;2, 1981.

Hoor, P., Fischer, H., Fischer, H., Fischer, H., Fischer, H., Lange, L., Lelieveld, J., and Brunner, D.: Seasonal variations of a mixing layer in the lowermost stratosphere as identified by the CO-O3 correlation from in situ measurements, Journal of Geophysical Research, https://doi.org/10.1029/2000jd000289, 2002.

Hoor, P., Gurk, C., Brunner, D., Hegglin, M. I., Wernli, H., Fischer, H., Fischer, H., Fischer, H., and Fischer, H.: Seasonality and extent of extratropical TST derived from in-situ CO measurements during SPURT, Atmospheric Chemistry and Physics, https://doi.org/10.5194/acp-4-1427-2004, 2004.

Höpfner, M., Ungermann, J., Borrmann, S., Wagner, R., Spang, R., Riese, M., Stiller, G., Appel, O., Batenburg, A. M., Bucci, S., Cairo, F., Dragoneas, A., Friedl-Vallon, F., Hünig, A., Johansson, S., Krasauskas, L., Legras, B., Leisner, T., Mahnke, C., Möhler, O., Molleker, S., Müller, R., Neubert, T., Orphal, J., Preusse, P., Rex, M., Saathoff, H., Stroh, F., Weigel, R., and Wohltmann, I.: Ammonium nitrate particles formed in upper troposphere from ground ammonia sources during Asian monsoons, Nature Geoscience, 12, 608–612, https://doi.org/10.1038/s41561-019-0385-8, 2019.

Institute of Volcanology and Seismology FEB RAS: VONA/KVERT Information Release, http://www.kscnet.ru/ivs/kvert/van/?n=2023-161, 2023.

Jaenicke, R.: Atmospheric aerosols and global climate, Journal of Aerosol Science, 11, 577–588, https://doi.org/10.1016/0021-8502(80)90131-7, 1980.

Junge, C. E. and Manson, J. E.: Stratospheric aerosol studies, Journal of Geophysical Research, 66, 2163–2182, https://doi.org/10.1029/JZ066i007p02163, 1961.

Jurkat, T., Voigt, C., Arnold, F., Schlager, H., Aufmhoff, H., Schmale, J., Schneider, J., Lichtenstern, M., and Dörnbrack, A.: Airborne stratospheric ITCIMS measurements of SO 2 , HCl, and HNO 3 in the aged plume of volcano Kasatochi, Journal of Geophysical Research, 115, D00L17, https://doi.org/10.1029/2010JD013890, 2010.

Jurkat, T., Kaufmann, S., Voigt, C., Schäuble, D., Jeßberger, P., and Ziereis, H.: The airborne mass spectrometer AIMS – Part 2: Measurements of trace gases with stratospheric or tropospheric origin in the UTLS, Atmospheric Measurement Techniques, 9, 1907–1923, https://doi.org/10.5194/amt-9-1907-2016, 2016.

Kaluza, T., Kunkel, D., and Hoor, P.: Composite analysis of the tropopause inversion layer in extratropical baroclinic waves, Atmospheric Chemistry and Physics, 19, 6621–6636, https://doi.org/10.5194/acp-19-6621-2019, 2019.

Kaluza, T., Kunkel, D., and Hoor, P.: On the occurrence of strong vertical wind shear in the tropopause region: a 10-year ERA5 northern hemispheric study, Weather and Climate Dynamics, 2, 631–651, https://doi.org/10.5194/wcd-2-631-2021, 2021.

Konopka, P. and Pan, L. L.: On the mixing-driven formation of the Extratropical Transition Layer (ExTL), Journal of Geophysical Research: Atmospheres, 117, n/a–n/a, https://doi.org/10.1029/2012jd017876, 2012.

Kremser, S., Thomason, L. W., von Hobe, M., Hermann, M., Deshler, T., Timmreck, C., Toohey, M., Stenke, A., Schwarz, J. P., Weigel, R., Fueglistaler, S., Prata, F. J., Vernier, J.-P., Schlager, H., Barnes, J. E., Antuña-Marrero, J.-C., Fairlie, D., Palm, M., Mahieu, E., Notholt, J., Rex, M., Bingen, C., Vanhellemont, F., Bourassa, A., Plane, J. M. C., Klocke, D., Carn, S. A., Clarisse, L., Trickl, T., Neely, R., James, A. D., Rieger, L., Wilson, J. C., and Meland, B.: Stratospheric aerosol-Observations, processes, and impact on climate, Reviews of Geophysics, 54, 278–335, https://doi.org/10.1002/2015rg000511, 2016.

Krüger, O. O., Holanda, B. A., Chowdhury, S., Pozzer, A., Walter, D., Pöhlker, C., Andrés Hernández, M. D., Burrows, J. P., Voigt, C., Lelieveld, J., Quaas, J., Pöschl, U., and Pöhlker, M. L.: Black carbon aerosol reductions during COVID-19 confinement quantified by aircraft measurements over Europe, Atmospheric Chemistry and Physics, 22, 8683–8699, https://doi.org/10.5194/acp-22-8683-2022, 2022.

Kunkel, D., Hoor, P., Kaluza, T., Ungermann, J., Kluschat, B., Giez, A., Lachnitt, H.-C., Kaufmann, M., and Riese, M.: Evidence of small-scale quasi-isentropic mixing in ridges of extratropical baroclinic waves, Atmospheric Chemistry and Physics, https://doi.org/10.5194/acp-19-12607-2019, 2019.

Marsing, A.: Chlorine partitioning in the lowermost Arctic stratosphere during winter – an aircraft in situ measurement perspective, Ph.D. thesis, 2021.

Marsing, A., Jurkat-Witschas, T., Grooß, J.-U., Kaufmann, S., Heller, R., Engel, A., Hoor, P., Krause, J., and Voigt, C.: Chlorine partitioning in the lowermost Arctic vortex during the cold winter 2015/2016, Atmospheric Chemistry and Physics, 19, 10 757–10 772, https://doi.org/10.5194/acp-19-10757-2019, 2019.

460   Martinsson, B. G.: Characteristics and origin of lowermost stratospheric aerosol at northern midlatitudes under volcanically quiescent conditions based on CARIBIC observations, Journal of Geophysical Research, 110, D12 201, https://doi.org/10.1029/2004JD005644, 2005.

Martinsson, B. G., Friberg, J., Sandvik, O. S., Hermann, M., van Velthoven, P. F. J., and Zahn, A.: Formation and composition of the UTLS aerosol, npj Climate and Atmospheric Science, 2, 40, https://doi.org/10.1038/s41612-019-0097-1, 2019.

465   Middlebrook, A. M., Bahreini, R., Bahreini, R., Bahreini, R., Jimenez, J. L., and Canagaratna, M. R.: Evaluation of Composition-Dependent Collection Efficiencies for the Aerodyne Aerosol Mass Spectrometer using Field Data, Aerosol Science and Technology, https://doi.org/10.1080/02786826.2011.620041, 2012.

Murphy, D. M., Froyd, K. D., Schwarz, J. P., and Wilson, J. C.: Observations of the chemical composition of stratospheric aerosol particles, Quarterly Journal of the Royal Meteorological Society, 140, 1269–1278, https://doi.org/10.1002/qj.2213, 2013.

470   Proffitt, M. H., Powell, J. A., Tuck, A. F., Fahey, D. W., Kelly, K. K., Krueger, A. J., Schoeberl, M. R., Gary, B. L., Margitan, J. J., Chan, K. R., Loewenstein, M., and Podolske, J. R.: A chemical definition of the boundary of the Antarctic ozone hole, Journal of Geophysical Research: Atmospheres, 94, 11 437–11 448, https://doi.org/10.1029/jd094id09p11437, 1989.

Re3data.Org: HALO database, https://doi.org/10.17616/R39Q0T, 2016.

Reifenberg, S. F., Martin, A., Kohl, M., Bacer, S., Hamryszczak, Z., Tadic, I., Röder, L., Crowley, D. J., Fischer, H., Kaiser, K., Schneider,
475   J., Dörich, R., Crowley, J., Tomsche, L., Marsing, A., Voigt, C., Zahn, A., Pöhlker, C., Holanda, B. A., Krüger, O. O., Pöschl, U., Pöhlker, M. L., Jöckel, P., Dorf, M., Schumann, U., Williams, J., Bohn, B., Curtius, J., Harder, H., Schlager, H., Lelieveld, J., and Pozzer, A.: Numerical simulation of the impact of COVID-19 lockdown on tropospheric composition and aerosol radiative forcing in Europe, Atmospheric Chemistry and Physics, https://doi.org/10.5194/acp-22-10901-2022, 2022.

Röder, L. L., Ort, L., Lelieveld, J., and Fischer, H.: Determination of Temporal Stability and Instrument Performance of an airborne QCLAS
480   via Allan-Werle-plots, https://doi.org/10.21203/rs.3.rs-3619758/v1, pREPRINT (Version 1) available at Research Square, 2023.

Rollins, A. W., Thornberry, T. D., Watts, L. A., Yu, P., Rosenlof, K. H., Mills, M., Baumann, E., Giorgetta, F. R., Bui, T. V., Höpfner, M., Walker, K. A., Boone, C., Bernath, P. F., Colarco, P. R., Newman, P. A., Fahey, D. W., and Gao, R. S.: The role of sulfur dioxide in stratospheric aerosol formation evaluated by using in situ measurements in the tropical lower stratosphere, Geophysical Research Letters, 44, 4280–4286, https://doi.org/10.1002/2017gl072754, 2017.

485   Schulz, C., Schneider, J., Holanda, B. A., Appel, O., Costa, A., de Sá, S. S., Dreiling, V., Fütterer, D., Jurkat-Witschas, T., Klimach, T., Krämer, M., Knote, C., Martin, S. T., Mertes, S., Pöhlker, M. L., Sauer, D., Voigt, C., Weinzierl, B., Ziereis, H., Walser, A., Zöger, M., Andreae, M. O., Artaxo, P., Machado, L. A. T., Pöschl, U., Wendisch, M., Borrmann, S., and Borrmann, S.: Aircraft-based observations of isoprene-epoxydiol-derived secondary organic aerosol (IEPOX-SOA) in the tropical upper troposphere over the Amazon region, Atmospheric Chemistry and Physics, https://doi.org/10.5194/acp-18-14979-2018, 2018.

490   Schumann, U., Bugliaro, L., Dörnbrack, A., Baumann, R., and Voigt, C.: Aviation Contrail Cirrus and Radiative Forcing Over Europe During 6 Months of COVID-19, Geophysical Research Letters, 48, https://doi.org/10.1029/2021gl092771, 2021a.

Schumann, U., Poll, I., Teoh, R., Koelle, R., Spinielli, E., Molloy, J., Koudis, G. S., Baumann, R., Bugliaro, L., Stettler, M., and Voigt, C.: Air traffic and contrail changes over Europe during COVID-19: a model study, Atmospheric Chemistry and Physics, 21, 7429–7450, https://doi.org/10.5194/acp-21-7429-2021, 2021b.

495 Seinfeld, J. H. and Pandis, S. N.: Atmospheric chemistry and physics: from air pollution to climate change, John Wiley & Sons, 2016.

Solomon, S., Daniel, J. S., Neely, R. R., Vernier, J.-P., Dutton, E. G., and Thomason, L. W.: The Persistently Variable "Background" Stratospheric Aerosol Layer and Global Climate Change, Science, 333, 866–870, https://doi.org/10.1126/science.1206027, 2011.

Sprenger, M. and Wernli, H.: The LAGRANTO Lagrangian analysis tool – version 2.0, Geoscientific Model Development, 8, 2569–2586, https://doi.org/10.5194/gmd-8-2569-2015, 2015.

500 Staehelin, J.: Ozone Measurements and Trends (Troposphere), in: Encyclopedia of Physical Science and Technology, pp. 539–561, Elsevier, https://doi.org/10.1016/b0-12-227410-5/00037-5, 2003.

Stein, A. F., Draxler, R. R., Rolph, G. D., Stunder, B. J. B., Cohen, M. D., and Ngan, F.: NOAA's HYSPLIT Atmospheric Transport and Dispersion Modeling System, Bulletin of the American Meteorological Society, 96, 2059–2077, https://doi.org/10.1175/bams-d-14-00110.1, 2015.

505 Tadic, I., Parchatka, U., Königstedt, R., and Fischer, H.: In-flight stability of quantum cascade laser-based infrared absorption spectroscopy measurements of atmospheric carbon monoxide, Applied Physics B, 123, 1–9, 2017.

Thouret, V., Thouret, V., Cammas, J.-P., Cammas, J.-P., Sauvage, B., Sauvage, B., Athier, G., Zbinden, R., Zbinden, R., Nédélec, P., Simon, P., and Karcher, F.: Tropopause referenced ozone climatology and inter-annual variability (1994–2003) from the MOZAIC programme, Atmospheric Chemistry and Physics, https://doi.org/10.5194/acp-6-1033-2006, 2005.

510 Tomsche, L., Marsing, A., Jurkat-Witschas, T., Lucke, J., Kaufmann, S., Kaiser, K., Schneider, J., Scheibe, M., Schlager, H., Röder, L. L., Fischer, H., Obersteiner, F., Zahn, A., Zöger, M., Lelieveld, J., and Voigt, C.: Enhanced sulfur in the upper troposphere and lower stratosphere in spring 2020, Atmospheric Chemistry and Physics, https://doi.org/10.5194/acp-22-15135-2022, 2022.

Voigt, C., Schumann, U., Jurkat, T., Schäuble, D., Schlager, H., Petzold, A., Gayet, J.-F., Krämer, M., Schneider, J., Borrmann, S., Schmale, J., Jessberger, P., Hamburger, T., Lichtenstern, M., Scheibe, M., Gourbeyre, C., Meyer, J., Kübbeler, M., Frey, W., Kalesse, H., Butler, 515 T., Lawrence, M. G., Holzäpfel, F., Arnold, F., Wendisch, M., Döpelheuer, A., Gottschaldt, K., Baumann, R., Zöger, M., Sölch, I., Rautenhaus, M., and Dörnbrack, A.: In-situ observations of young contrails – overview and selected results from the CONCERT campaign, Atmospheric Chemistry and Physics, 10, 9039–9056, https://doi.org/10.5194/acp-10-9039-2010, 2010.

Voigt, C., Jessberger, P., Jurkat, T., Kaufmann, S., Baumann, R., Schlager, H., Bobrowski, N., Giuffrida, G., and Salerno, G.: Evolution of CO2, SO2, HCl, and HNO3 in the volcanic plumes from Etna, Geophysical Research Letters, 41, 2196–2203, 520 https://doi.org/https://doi.org/10.1002/2013GL058974, 2014.

Voigt, C., Voigt, C., Lelieveld, J., Lelieveld, J., Schlager, H., Schlager, H., Schneider, J., Schneider, J., Curtius, J., Curtius, J., Meerkötter, R., Meerkötter, R., Sauer, D., Sauer, D., Bugliaro, L., Bugliaro, L., Bohn, B., Bohn, B., Crowley, J. N., Crowley, J. N., Erbertseder, T., Erbertseder, T., Groβ, S., Groβ, S., Hahn, V., Hahn, V., Li, Q., Li, Q., Mertens, M., Mertens, M., Pöhlker, M. L., Pöhlker, M. L., Pozzer, A., Pozzer, A., Schumann, U., Schumann, U., Tomsche, L., Tomsche, L., Williams, J., Williams, J., Zahn, A., Zahn, A., Andreae, M., 525 Andreae, M., Borrmann, S., Borrmann, S., Bräuer, T., Bräuer, T., Dörich, R., Dörich, R., Dörnbrack, A., Dörnbrack, A., Edtbauer, A., Edtbauer, A., Ernle, L., Ernle, L., Fischer, H., Fischer, H., Giez, A., Giez, A., Granzin, M., Granzin, M., Grewe, V., Grewe, V., Harder, H., Harder, H., Heinritzi, M., Heinritzi, M., Holanda, B. A., Holanda, B. A., Jöckel, P., Jöckel, P., Kaiser, K., Kaiser, K., Krüger, O. O., Krüger, O. O., Lucke, J., Lucke, J., Marsing, A., Marsing, A., Martin, A., Martin, A., Matthes, S., Matthes, S., Pöhlker, C., Pöhlker, C., Pöschl, U., Pöschl, U., Reifenberg, S., Reifenberg, S., Ringsdorf, A., Ringsdorf, A., Scheibe, M., Scheibe, M., Tadic, I., Tadic, I., Zauner-Wieczorek,

530   M., Zauner-Wieczorek, M., Henke, R., Henke, R., Rapp, M., and Rapp, M.: Cleaner skies during the COVID-19 lockdown, Bulletin of
         the American Meteorological Society, https://doi.org/10.1175/bams-d-21-0012.1, 2022.

         Williamson, C. J., Kupc, A., Rollins, A., Kazil, J., Froyd, K. D., Ray, E. A., Murphy, D. M., Schill, G. P., Peischl, J., Thompson, C., Bourgeois,
         I., Ryerson, T. B., Diskin, G. S., DiGangi, J. P., Blake, D. R., Bui, T. P. V., Dollner, M., Weinzierl, B., and Brock, C. A.: Large hemispheric
         difference in nucleation mode aerosol concentrations in the lowermost stratosphere at mid- and high latitudes, Atmospheric Chemistry

535   and Physics, 21, 9065–9088, https://doi.org/10.5194/acp-21-9065-2021, 2021.

         Zahn, A., Brenninkmeijer, C. A. M., and van Velthoven, P. F. J.: Passenger aircraft project CARIBIC 1997-2002, Part I: the extratropical
         chemical tropopause, Atmospheric Chemistry and Physics, https://doi.org/10.5194/acpd-4-1091-2004, 2004.

         Zahn, A., Weppner, J., Widmann, H., Schlote-Holubek, K., Burger, B., Kühner, T., Franke, H., Franke, H., and Franke, H.: A
         fast and precise chemiluminescence ozone detector for eddy flux and airborne application, Atmospheric Measurement Techniques,

540   https://doi.org/10.5194/amt-5-363-2012, 2011.